PV and Wind Energy Conversion Exploration based on Grid Integrated Hybrid Generation Using the Cuttlefish Algorithm

Y. Nagaraja
Department of EEE
Annamacharya Institute of Technology and Sciences
Kadapa, India
nagarajaeps@gmail.com

T. Devaraju
Department of EEE
Sree Vidyanikethan Engineering College (Autonomous)
Tirupathi, India
devaraj_t@yahoo.com

A. Muni Sankar
Department of EEE
Sree Rama Engineering College
Tirupathi, India
naac.co-ordinator@sreerama.ac.in

V. Narasimhulu
Department of EEE
Rajeev Gandhi Memorial College of Engineering and Technology (Autonomous), Nandyal, India
narasimhapid@gmail.com

Received: 22 September 2022 | Revised: 28 September 2022 | Accepted: 1 October 2022

Abstract-This paper focuses on the exploration of grid integrated hybrid generation comprising of Photovoltaic (PV) and Wind Energy Conversion Systems (WECSs) using the Cuttlefish Algorithm (CFA). PV and wind energies are opposite because sunny days are normally calm, and strong winds frequently occur on cloudy days or at night. Hence, a hybrid PV and wind power system is more reliable than either individual source in terms of delivering uninterrupted power. The regulation of the DC voltage is the key issue in this configuration. The conventional PI controller is inaccurate in regulating the DC voltage. The PI controller gain tuning using optimization techniques provides good DC voltage regulation and less Total Harmonic Distortion (THD). Hence, CFA is proposed for the tuning of PI gains. The performance parameters such as DC voltage regulation and THD of CFA are analyzed.

Keywords-photovoltaic; wind energy conversion system; PWM; PI; AWT; PR; PSO; CFA

I. INTRODUCTION

The quick advancement of power electronics has increased the amount of solar and wind energy applications. Solar energy and wind energy are generally considered to be incompatible with one another due to the fact that calm winds are more typical on cloudy days or at night, whereas sunny days typically include calm conditions. As a result, a hybrid PV and wind power system is more reliable than any independent source in terms of delivering continuous electricity. Conventionally, a large energy storing battery bank [1] is adopted to reliably supply power and maximize power from PV arrays or wind turbines [1, 18], both of which are intermittent. The battery is not an environmentally friendly product, it is expensive, has a limited life cycle, it is large and heavy [2], and, pollutes the environment with chemical waste. As a consequence, it is fairly usual practice to link renewable energy sources like solar or wind to the main power grid directly. The integration of wind and solar power hybrids into the grid system is an area that is explored in this study.

II. MODELING OF THE HYBRID GENERATION SYSTEM

The structure of the projected PV and wind based hybrid renewable generation power system is depicted in Figure 1 and its comprehensive stipulations are listed in Table I [3].

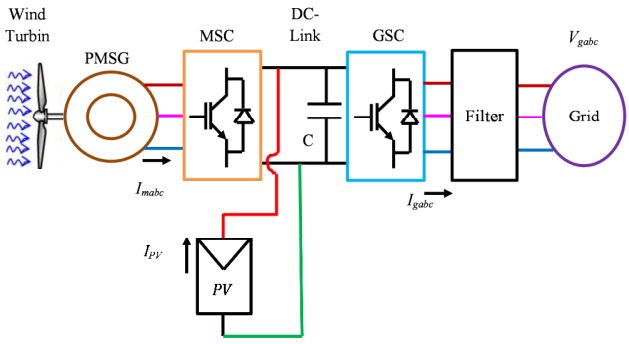

Fig. 1. Schematic representation of a hybrid generation system connected to the grid.

The block diagram of the hybrid renewable generation power system including WEC, PV, inverter, and grid is depicted in Figure 1. The wind energy based power is

Corresponding author: Y. Nagaraja

converted to the dc supply and then the PV supply is integrated [4]. The combined voltage at the dc link is converted to ac supply using a standard inverter for the integration of the ac power grid. The filter is used between the inverter and the grid for obtaining quality signal. Two converters are brought together to form a back-to-back converter. The connection between a Grid Side Converter (GSC) and a Machine Side Converter is made via a DC-bus capacitor (MSC) [3]. The vector control method is utilized so that the VSI can be controlled. The vector control is constructed using two different loops. The first loop is responsible for regulating the DC-link voltage and the second loop is in charge of controlling the amount of the current that is injected. When compared to the voltage loop, the current loop is intended to react more quickly to any disturbance that may occur [3].

Wind turbines generate mechanical power by capturing wind [11], as shown in (1):

$$P_m = \frac{1}{2}\pi\rho R^2 C_P(\beta,\lambda)v^3 \quad (1)$$

where R and ρ denote the radius of blades and air density, β is the pitch angle, and λ the tip-speed ratio. The wind speed is denoted by v. C_p represents the utilization coefficient of wind energy [11]. Equation (2) expresses the wind turbine mechanical acting torque [11]:

$$T_m = \frac{P_m}{\omega_m} = \frac{1}{2}\pi\rho R^3 C_P(\beta,\lambda)\, v^2/\lambda \quad (2)$$

where $\omega_m = \frac{R}{\lambda v}$ denotes the mechanical angular velocity. The PMSG is a type of power conversion machinery that converts mechanical energy to electrical energy. The Park transformation, also known as dq transformation, is used to transform the time varying quantities into DC quantities.

Equations (3) and (4) present the voltage expression of PMSG in a 2-phase rotating d-q axis system [3]:

$$L_{sd}\frac{dI_{sd}}{dt} = -R_s I_{sd} + \omega_e L_{sq} I_{sq} + V_{sd} \quad (3)$$

$$L_{sq}\frac{dI_{sq}}{dt} = -R_s I_{sq} - \omega_e L_{sd} I_{sd} - \omega_e \psi + V_{sq} \quad (4)$$

where V_{sd} and V_{sq} are the stator voltages in the d-q components and I_{sd} and I_{sq} are the d and q current components in the rotor flux. The stator resistance is denoted by R_s. L_{sd} and L_{sq} are the equal inductances of stator d-q axis in the surface mounted PMSG. ω_e and ψ denote the electrical angular speed and permanent magnet chain respectively.

Equation (5) represents the electromagnetic torque of PMSG [11]:

$$T_e = 1.5 n_p[(L_{sd} - L_{sq})I_{sd}I_{sq} + \psi I_{sq}] \quad (5)$$

Equation (6) expresses the mechanical properties of a system that employs a dynamic one-mass model:

$$T_m = J\frac{d\omega_m}{dt} + B\omega_m + T_e \quad (6)$$

The transmission system's moment of inertia and the coefficient of self-damping are denoted by J and B respectively.

The PV array is depicted in Figure 1, where N_s represents the number of cells connected in series and N_p the number of modules connected in parallel. In this particular instance, the array denoted by I_{pv} can be written as:

$$I_{pv} = N_P I_P - N_P I_s\left[exp\left[\alpha\left(\frac{V_{PV}}{N_s} + \frac{R_s I_{PV}}{N_P}\right)\right] - 1\right] - \frac{N_P}{R_{sh}}\left(\frac{V_{PV}}{N_s} + \frac{R_s I_{PV}}{N_P}\right) \quad (7)$$

Considering zero sequence components in a 3-phase system is not necessary because there is no circulation path. Equation (8) depicts the three-phase balanced voltage:

$$\begin{bmatrix} V_{ga} \\ V_{gb} \\ V_{gc} \end{bmatrix} = V_m \begin{bmatrix} \sin\omega t \\ \sin(\omega t + 120^0) \\ \sin(\omega t - 120^0) \end{bmatrix} \quad (8)$$

Control systems make it possible to improve the effectiveness as well as the quality of the electricity that is generated by a wind energy conversion system. They are closed-loop feedback systems that control switching elements in active power conversion stages. Initially, the rotational speed of the generator can be sensed and controlled using an active rectifier and a Proportional Integral (PI) controller. Also, the grid-side inverter PWM signal can be used to regulate the system. It can be adopted to keep the DC link at a constant voltage [13-17], which will decouple the grid from power fluctuations caused by wind variations.

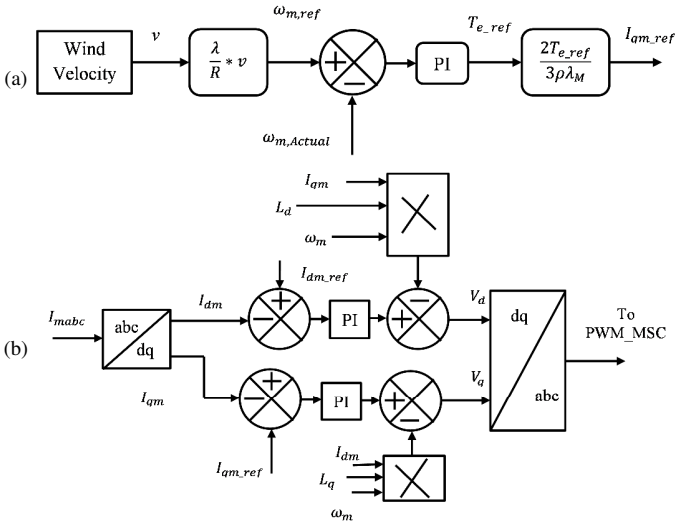

Fig. 2. Overall control block illustration for MSC. (a) Reference generation of I_q, (b) Control block illustration.

The overall control method for the PMSG [1, 4, 9-12] based wind energy power system is depicted in Figure 2. The reference torque is generated in a torque control scheme by measuring the generator speed. The Park transformation is used to convert the measured 3-phase current in the stator into a d-q component. Thus, the stator current is equal to the q-axis component. Thus, torque is controlled by only changing the stator current in the q-axis direction. It is determined whether the measured d-q stator currents are greater than the reference

d-q currents in the stator, and the difference is connected to the PI controllers [8], which produce the stator reference voltages in the d-q components. The reference voltages in stator of d-q components are transformed to the reference 3-phase stator voltages V_a, V_b, and V_c and are sent to the PWM, which generates the converter switching pulses.

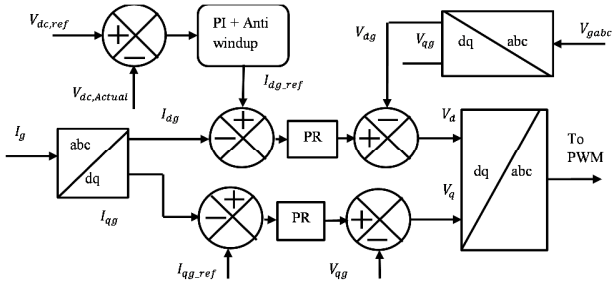

Fig. 3. Control block diagram of the GSC.

The GSC's role is to ensure that the dc-link voltage stays the same all the time [5]. Figure 3 depicts the block diagram of the control of GSC. The current reference (I_{dg_ref}) is generated using the PI+AWT method. The GSC output current is converted from abc signal to dq signal and the components of this current are compared with the reference currents I_{dg_ref} and I_{qg_ref}. This design is made up of one outer voltage loop and two inside current loops, which are connected. The dc-link voltage loop provides the reference d-axis component of grid current. It is necessary to match the reference and measured dc-link voltages, and vector control is used to handle errors. The reference d-axis grid current is produced by the PI+AWT controller. The inner Proportional-Resonant (PR) controller produces the d-q axis grid voltage from the d-axis reference grid current and the actual d-axis grid current. Park transformation is adopted to convert the d-q voltage components into natural abc grid components. The actual 3-phase abc grid voltage components are then sent to the PWM generator, which generates the firing pulses to the VSC. Figure 4 depicts the PR controller's block diagram. The PR control method has a high gain at the resonant frequency, which ensures that a little steady-state inaccuracy is presented between the actual and the reference signal. The PR controller is composed of a proportional and a resonant term.

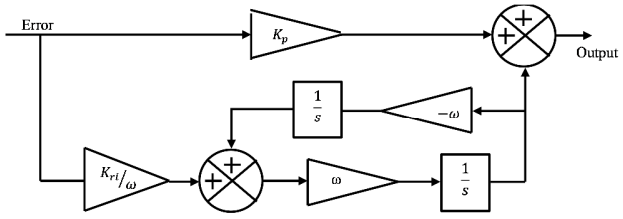

Fig. 4. Block diagram of the PR current controller.

III. CUTTLEFISH OPTIMIZATION SCHEME

Cuttlefish is a species of mollusk and it is well-known for its ability to change color in such a way that it either blends in with its surroundings or puts on a spectacular show. The program is designed to function in a manner analogous to the color-changing systems that are present in cuttlefish. The patterns and colors that can be observed on cuttlefish are the result of light being reflected off of the several layers of cells within the animal, including chromatophores, leucophores, and iridophores. Reflection and visibility are both taken into consideration by the CFA as important activities. The visibility process replicates the visibility of matching patterns, whereas the reflection process models the mechanism that controls how the light is reflected. The patterns and colors that may be seen in cuttlefish are the results of light being reflected from multiple layers of cells. The complete steps of the CFO algorithm are depicted in the flowchart of Figure 5.

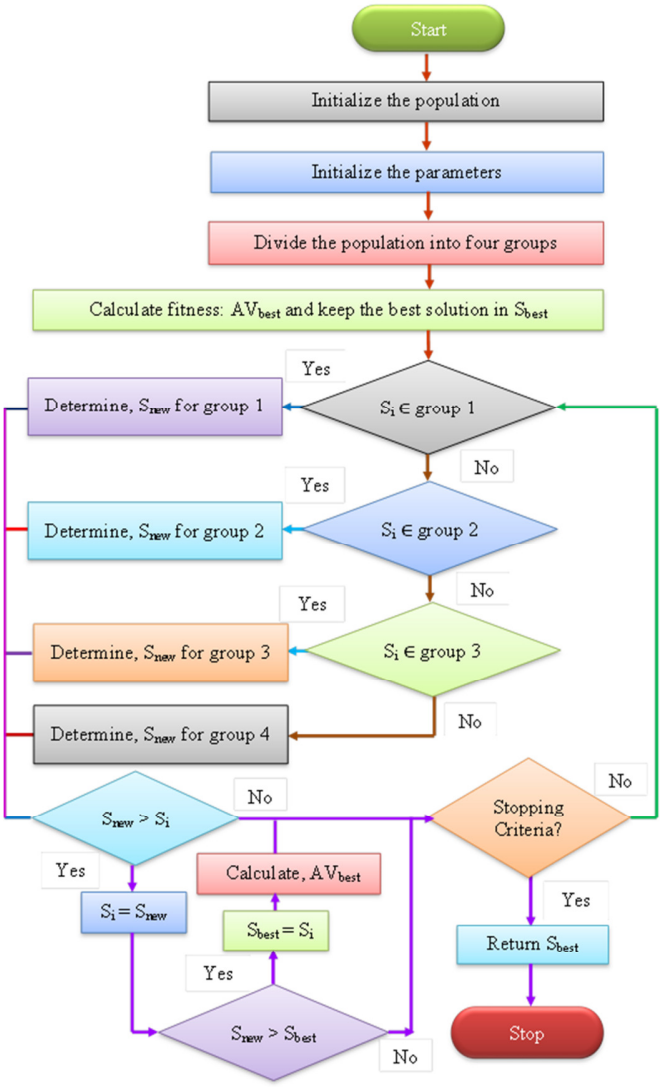

Fig. 5. Flowchart of the CFO algorithm.

IV. SIMULATION RESULTS AND DISCUSSION

The performance of proposed grid-connected HRES is analyzed using the MATLAB simulation results. The proposed work was simulated in 4 cases: constant wind speed and

irradiation, variable wind speed and constant irradiation, constant wind speed and variable irradiation, and variable wind speed and variable irradiation. The PR controller was adopted as the current controller. The CFA was adopted for dc voltage regulation and its performance was compared with conventional controllers', such as the AWT controller and the PSO algorithm. The simulation parameters are listed in Table I [7].

TABLE I. SIMULATION PARAMETERS

Description	Value
PMSM parameters	
Stator phase resistance *Rs*	2.8750Ω
Ld (H), *Lq*(H)	8.5mH, 8.5mH
Inertia (kg.m^2)	0.0019
Friction factor (N.m.s)	0.001
No. of poles	4
Flux linkage	0.175 v.s
DC link parameters	
DC link capacitor	4700 µF
Reference DC voltage	800V
GSC parameters	
Switches	IGBT
Switching frequency	7000Hz
Filter inductance	6 mH
Grid parameters	
Voltage	400V (r.m.s)
Frequency	50 Hz
Source resistance	0.01Ω
Source inductance	2µH
Turbine parameters	
Reference wind speed	12m/s
Reference voltage	1.2 p.u
PV Parameters	
Open Circuit Voltage V_{oc}	43.5 V
Short Circuit Current I_{sc}	2.783 A

A. Case 1: Constant Wind Speed and Irradiation

In this case, the wind speed value was set at 12m/s and the PV irradiation was maintained constant and equal to 1000W/m^2 throughout the simulation as shown in Figures 6 and 7 respectively.

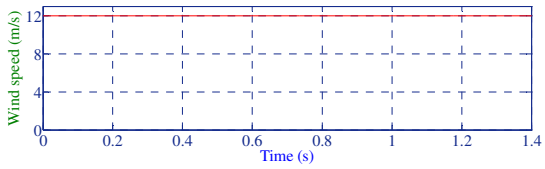

Fig. 6. Constant wind speed.

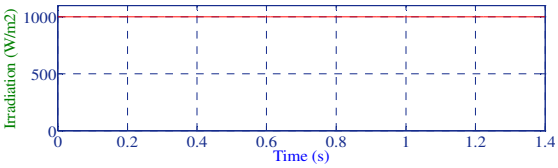

Fig. 7. Constant PV irradiation.

The CFA response curves are presented in Figure 8. The DC link voltage when using the CFA algorithm has a value of 800V and it is tracking the reference voltage after 0.06s. All the grid voltages are sinusoidal in nature and balanced. The response curves of the grid voltage and current are also presented in Figure 8.

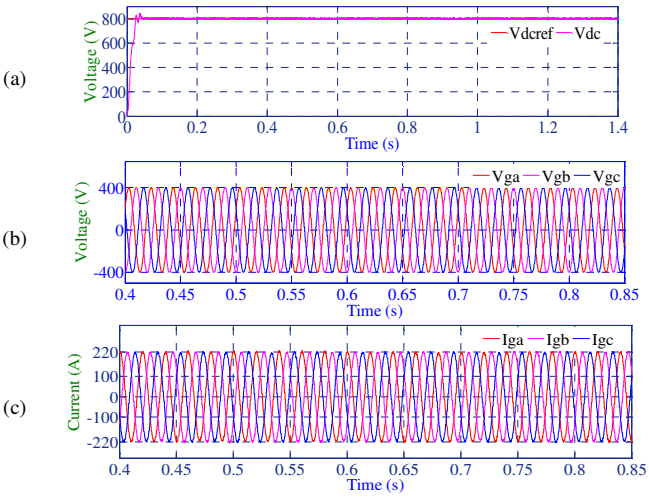

Fig. 8. Response curves of CFA (case 1): (a) DC link Voltage, (b) grid Voltage, (c) grid current.

B. Case 2: Variable Wind Speed and Constant Irradiation

In this case, the variable wind speed depicted in Figure 9 was applied. The wind speed was 12m/s from 0 to 0.2s, it reduced to 8m/s at 0.2s, changed to 10m/s at 0.5sec, and changed back to the initial value at 0.8s.

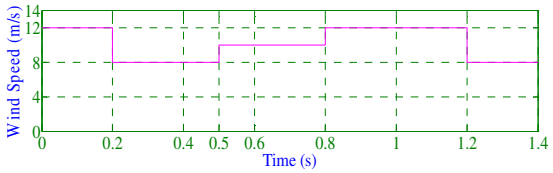

Fig. 9. Variable wind speed.

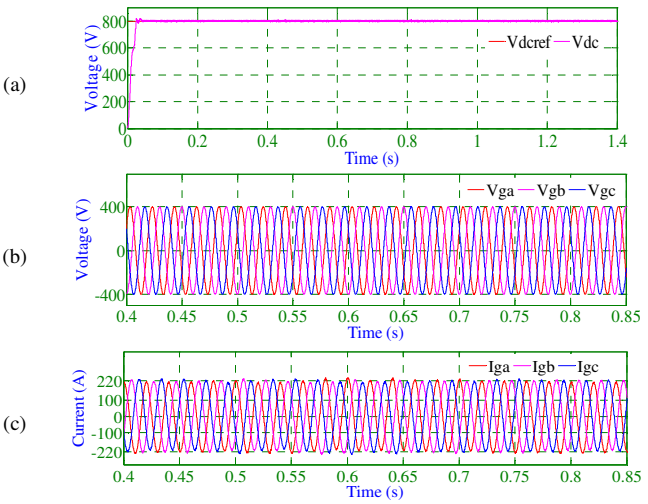

Fig. 10. Response curves of CFA (case 2): (a) DC link Voltage, (b) grid Voltage, (c) grid current.

The response curves using CFO are presented in Figure 10. The DC link voltage using the CFA algorithm has a value of 800V and it is tracking the reference voltage after 0.06s. All the grid voltages are in sinusoidal nature and balanced. The response curves of the grid voltage and current are also presented in Figure 10.

C. Case 3: Constant Wind Speed and Variable Irradiation

In this case, the change of PV irradiation is applied as illustrated in Figure 11. A constant irradiation of 1000W/m^2 is applied from 0 to 0.5s, it is then reduced to 700W/m^2, and is again 1000W/m^2 at 0.8s. The response curves using CFO are presented in Figure 12. The DC link voltage using CFA algorithm has a value of 800V and it is tracking the reference voltage after 0.06s as depicted in Figure 12(a). All the grid voltages are sinusoidal in nature and balanced. The response curves of grid voltage and current are also presented in Figure 12.

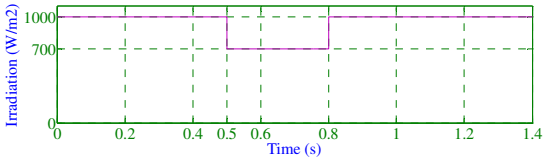

Fig. 11. Variable PV irradiation.

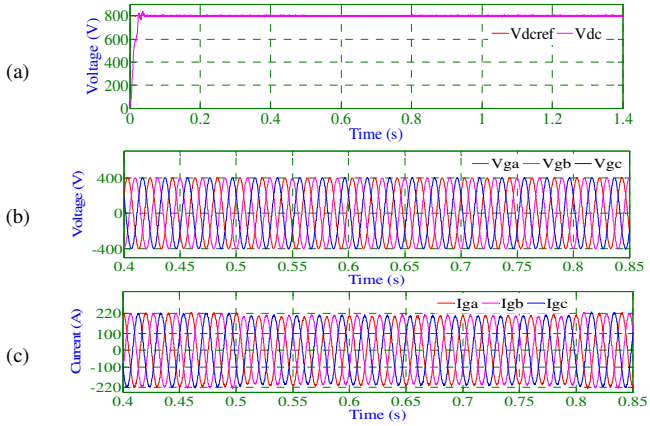

Fig. 12. Response curves of CFA (case 3): (a) DC link Voltage, (b) grid Voltage, (c) grid current.

D. Case 4: Variable Wind Speed and Variable Irradiation

In this case, variable wind speed as depicted in Figure 6 and variable PV irradiation as illustrated in Figure 11 are applied. The response curves using CFO are presented in Figure 13. The DC link voltage using CFO algorithm has a value of 800V and it is tracking the reference voltage after 0.06s as depicted in Figure 13. All the grid voltages are sinusoidal in nature and balanced. The response curves of grid voltage and current are also presented in Figure13.

Further, comparative performance analysis was conducted with THD. The FFT spectrum using the PI+AWT controller, the PSO algorithm, and CFA are presented in Figure 14. The THD when using the PI+AWT controller, PSO, and CFA is 1.97%, 1.62%, and 1.56% respectively. The proposed controller (CFA) performed better than the PI+AWT controller and the PSO algorithm. The comparative performance indices are listed in Table II. It is observed that the CFA has performed well in regulating the dc voltage. The dc voltage reached the reference voltage at 0.04s which is less compared than the time it took in both PI+AWT and PSO.

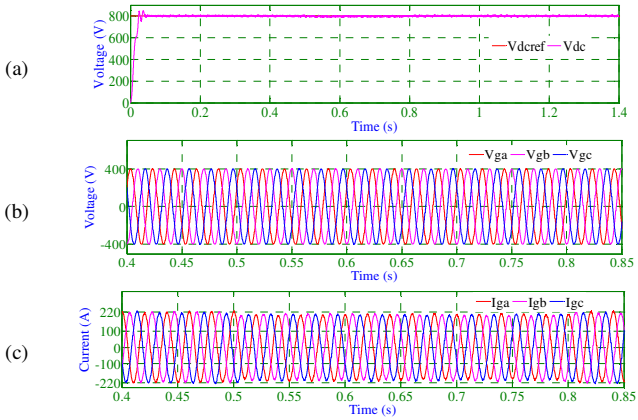

Fig. 13. Response curves of CFA (case 4): (a) DC link Voltage, (b) grid Voltage, (c) grid current.

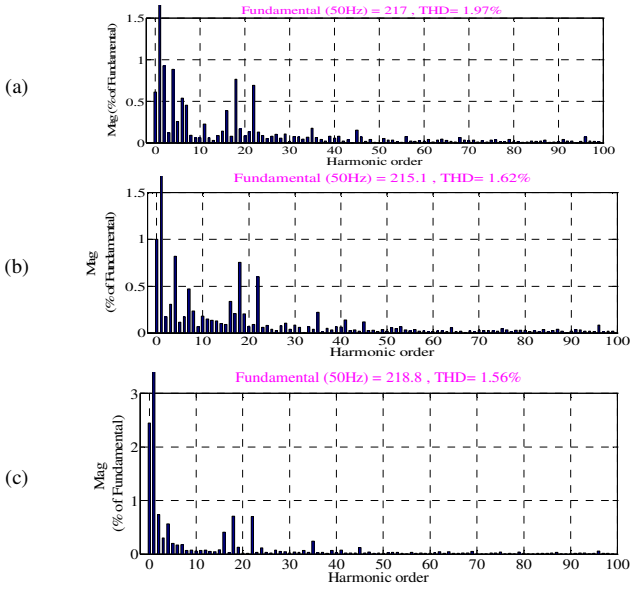

Fig. 14. THD comparison. FFT spectrum of grid current using (a) AWT controller, (b) PSO algorithm, (c) CFA.

TABLE II. PERFORMANCE COMPARISON

Controller	DC voltage settling time (s)	%THD in current signal
AWT	0.15	1.97
PSO	0.1	1.62
CFA	0.04	1.56

V. CONCLUSION

The concept of hybrid solar and wind power generation was described in detail in this paper, and the training procedure of a

CFA-based optimization algorithm is presented. From the results, it is realized that the CFA performed better than PI+AWT and PSO. Optimum DC voltage regulation is achieved with the use of the CFA algorithm. In order to demonstrate the applicability of the suggested controller, simulations were carried out in MATLAB/SIMULINK.

REFERENCES

[1] Y.-M. Chen, Y.-C. Liu, S.-C. Hung, and C.-S. Cheng, "Multi-Input Inverter for Grid-Connected Hybrid PV/Wind Power System," *IEEE Transactions on Power Electronics*, vol. 22, no. 3, pp. 1070–1077, Feb. 2007, https://doi.org/10.1109/TPEL.2007.897117.

[2] J. B. V. Subrahmanyam, P. Alluvada, Bandana, K. Bhanupriya, and C. Shashidhar, "Renewable Energy Systems: Development and Perspectives of a Hybrid Solar-Wind System," *Engineering, Technology & Applied Science Research*, vol. 2, no. 1, pp. 177–181, Feb. 2012, https://doi.org/10.48084/etasr.104.

[3] A. F. Tazay, A. M. A. Ibrahim, O. Noureldeen, and I. Hamdan, "Modeling, Control, and Performance Evaluation of Grid-Tied Hybrid PV/Wind Power Generation System: Case Study of Gabel El-Zeit Region, Egypt," *IEEE Access*, vol. 8, pp. 96528–96542, 2020, https://doi.org/10.1109/ACCESS.2020.2993919.

[4] A. V. P. Kumar, A. M. Parimi, and K. U. Rao, "Investigation of small PMSG based wind turbine for variable wind speed," in *2015 International Conference on Recent Developments in Control, Automation and Power Engineering (RDCAPE)*, Noida, India, Mar. 2015, pp. 107–112, https://doi.org/10.1109/RDCAPE.2015.7281378.

[5] N. A. Orlando, M. Liserre, R. A. Mastromauro, and A. Dell'Aquila, "A Survey of Control Issues in PMSG-Based Small Wind-Turbine Systems," *IEEE Transactions on Industrial Informatics*, vol. 9, no. 3, pp. 1211–1221, Dec. 2013, https://doi.org/10.1109/TII.2013.2272888.

[6] G. Mustafa, M. H. Baloch, S. H. Qazi, S. Tahir, N. Khan, and B. A. Mirjat, "Experimental Investigation and Control of a Hybrid (PV-Wind) Energy Power System," *Engineering, Technology & Applied Science Research*, vol. 11, no. 1, pp. 6781–6786, Feb. 2021, https://doi.org/10.48084/etasr.3964.

[7] W. M. Amutha, Renugadevi, and V. Rajini, "A Novel Fused Converter for Hybrid Power Systems," *Advanced Materials Research*, vol. 984–985, pp. 744–749, 2014, https://doi.org/10.4028/www.scientific.net/AMR.984-985.744.

[8] J. Biela, D. Hassler, J. Schönberger, and J. W. Kolar, "Closed-Loop Sinusoidal Input-Current Shaping of 12-Pulse Autotransformer Rectifier Unit With Impressed Output Voltage," *IEEE Transactions on Power Electronics*, vol. 26, no. 1, pp. 249–259, Jan. 2011, https://doi.org/10.1109/TPEL.2010.2052633.

[9] X. Zeng, T. Liu, S. Wang, Y. Dong, and Z. Chen, "Comprehensive Coordinated Control Strategy of PMSG-Based Wind Turbine for Providing Frequency Regulation Services," *IEEE Access*, vol. 7, pp. 63944–63953, 2019, https://doi.org/10.1109/ACCESS.2019.2915308.

[10] M. Benchagra, M. Maaroufi, and M. Ouassaid, "Study and analysis on the control of SCIG and its responses to grid voltage unbalance," in *2011 International Conference on Multimedia Computing and Systems*, Ouarzazate, Morocco, Apr. 2011, pp. 1–5, https://doi.org/10.1109/ICMCS.2011.5945737.

[11] J. Liu, C. Zhao, and Z. Xie, "Power and Current Limiting Control of Wind Turbines Based on PMSG Under Unbalanced Grid Voltage," *IEEE Access*, vol. 9, pp. 9873–9883, 2021, https://doi.org/10.1109/ACCESS.2021.3049839.

[12] A. Mittal and L. Taylor, "Optimization of Large Wind Farms Using a Genetic Algorithm," in *ASME 2012 International Mechanical Engineering Congress and Exposition*, Houston, TX, USA, Nov. 2012, vol. 7, https://doi.org/10.1115/IMECE2012-87816.

[13] V. Narasimhulu, D. V. Ashok Kumar, and Ch. Sai Babu, "Computational intelligence based control of cascaded H-bridge multilevel inverter for shunt active power filter application," *Journal of Ambient Intelligence and Humanized Computing*, Jan. 2020, https://doi.org/10.1007/s12652-019-01660-0.

[14] V. Narasimhulu, D. V. Ashok Kumar, and Ch. Sai Babu, "Fuzzy Logic Control of SLMMC-Based SAPF Under Nonlinear Loads," *International Journal of Fuzzy Systems*, vol. 22, no. 2, pp. 428–437, Mar. 2020, https://doi.org/10.1007/s40815-019-00622-0.

[15] M. Heidari, "Improve the Power Quality of Wind Power Plant by Modifying the Theory of Instantaneous Active and Reactive Power," *International Journal Of Renewable Energy Research*, vol. 5, no. 3, pp. 722–731, Sep. 2015.

[16] V. Narasimhulu, D. V. Ashok Kumar, and Ch. Sai Babu, "Recital analysis of multilevel cascade H-bridge based active power filter under load variation," *SN Applied Sciences*, vol. 1, no. 12, Nov. 2019, Art. no. 1621, https://doi.org/10.1007/s42452-019-1669-8.

[17] V. Narasimhulu and K. Jithendra Gowd, "Performance Analysis of Single-Stage PV Connected Three-Phase Grid System Under Steady State and Dynamic Conditions," in *Cybernetics, Cognition and Machine Learning Applications*, Singapore, 2021, pp. 39–46, https://doi.org/10.1007/978-981-33-6691-6_5.

[18] N. Regis, C. M. Muriithi, and L. Ngoo, "Optimal Battery Sizing of a Grid-Connected Residential Photovoltaic System for Cost Minimization using PSO Algorithm," *Engineering, Technology & Applied Science Research*, vol. 9, no. 6, pp. 4905–4911, Dec. 2019, https://doi.org/10.48084/etasr.3094.